

# Higgs gap modes in superconducting circuit quantisation

Yun-Chih Liao,<sup>1,2,\*</sup> Benjamin J. Powell,<sup>2</sup> and Thomas M. Stace<sup>1,2,†</sup>

<sup>1</sup>ARC Centre of Excellence for Engineered Quantum Systems

<sup>2</sup>School of Mathematics and Physics, The University of Queensland, Brisbane, Queensland 4072, Australia  
(Dated: March 10, 2026)

We extend a recently developed projective circuit quantisation approach to incorporate superconducting Higgs modes associated to gap dynamics. This approach starts from a microscopic fermionic Hamiltonian for mesoscopic superconductors, and projects the system onto a low-energy, multi-determinant ‘BCS’ Hilbert space. We derive analytical results for the superconducting Higgs mass, ‘spring’ constant, and oscillation frequency of the gap dynamics, which we validate numerically. We compute anharmonic corrections to the Higgs frequency for higher excitations of small superconducting islands, and compare our results to previous long-wavelength calculations.

The key to understanding superconductivity was the discovery of the complex order-parameter,  $\Delta \equiv \Delta e^{i\phi}$ . Two types of collective modes emerge: Nambu-Goldstone phase modes associated to dynamics of  $\phi$ , which is the foundational degree of freedom underpinning the theory of superconducting quantum circuits, and massive Higgs ‘gap’ modes associated to dynamics of  $\Delta$  [1–3], which is comparatively underexplored. The microscopic theory of superconductivity was established by Bardeen, Cooper and Schrieffer (BCS) to compute the equilibrium gap amplitude  $\Delta_{\text{BCS}}$  [4–7], as a central physical quantity.

The frequency of Higgs modes is predicted in Ginzburg-Landau (GL) mean-field theory to soften as the temperature  $T$  approaches the critical temperature,  $\omega_{\text{H}} \propto \sqrt{T_c - T}$  [8]. At long wavelength and  $T = 0$ , microscopic models indicate that  $\omega_{\text{H}} \approx 2\Delta_{\text{BCS}}$  [9–15]. Experimental observations of Higgs modes in superconductors are notably sparse due to weak electromagnetic coupling [16, 17], with some results for charge-density-waves [18, 19], and terahertz spectroscopy [20–22]. Bulk superconducting experiments, using non-equilibrium anti-Stokes Raman scattering [23], or quantum pathway interference [24], have reported  $\omega_{\text{H}} < 2\Delta_{\text{BCS}}$ .

In parallel, superconducting circuits are now important platforms for quantum processors. The underlying circuit theory quantises the GL phase angle  $\phi \in [-\pi, \pi)$  [25–27], implicitly assuming a fixed, mean-field amplitude,  $\Delta = \Delta_{\text{BCS}}$ . Practically, this has been very successful, but has some conceptual weaknesses [28, 29].

In this letter, we extend recent ‘first principles’ projective approaches that derive quantum circuit theory directly from a microscopic Hamiltonian [28, 29], to include gap dynamics in a unified quantum treatment of both  $\phi$  and  $\Delta$  in superconducting circuits. Our results yield estimates for the frequency and anharmonicity of gap-mode transitions for small superconducting islands.

We start from a microscopic electronic Hamiltonian for a small, isolated island of superconducting metal consisting of  $n$  electronic modes near half-filling,

$$\hat{H}_{\text{el}} = \sum_{\mathbf{k}s} \epsilon_{\mathbf{k}} c_{\mathbf{k}s}^\dagger c_{\mathbf{k}s} - |g|^2 \sum_{\mathbf{k}\mathbf{k}'} c_{\mathbf{k}\uparrow}^\dagger c_{-\mathbf{k}\downarrow}^\dagger c_{-\mathbf{k}'\downarrow} c_{\mathbf{k}'\uparrow} + E_F, \quad (1)$$

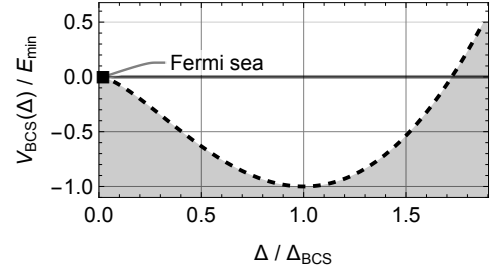


FIG. 1. The BCS potential (dashed), given by the diagonal part of the Hamiltonian function  $V_{\text{BCS}}(\Delta) \equiv H(\varphi = 0; \Delta, \Delta)$ . The energy is minimised at the BCS mean-field value  $\Delta = \Delta_{\text{BCS}}$ , where  $V_{\text{BCS}} = -E_{\text{min}} = -n\mathcal{B}e^{-2/\lambda}$ . The state at  $\Delta = 0$  is the zero-temperature Fermi sea.

where  $-\mathcal{B} < \epsilon_{\mathbf{k}} < \mathcal{B}$  is the single-electron kinetic energy for mode  $\mathbf{k}$  in the bandwidth  $\pm\mathcal{B}$ ,  $s \in \{\uparrow, \downarrow\}$ ,  $g$  is the effective electron-electron binding energy,  $c_{\mathbf{k}}^{(\dagger)}$  are electronic mode creation and annihilation operators, and  $E_F = n\mathcal{B}/2$ . The low-energy physics is controlled by the dimensionless material parameter  $\lambda = |g|^2 n / (2\mathcal{B}) \ll 1$ , which is independent of the system size  $n$  (since  $|g|^2 \propto 1/n$ ) [30].

We assume that the island is smaller than the coherence length, so that the low-energy subspace is spanned by a basis of BCS states parameterised by a complex parameter  $\Delta$ ,  $\mathcal{H}_{\text{BCS}} = \text{span}\{|\Psi(\Delta)\rangle\}_{\Delta \in S \subset \mathbb{C}}$ , where

$$|\Psi(\Delta)\rangle = \prod_{\mathbf{k}} (u_{\mathbf{k}}(\Delta) + v_{\mathbf{k}}(\Delta) e^{i\phi} c_{\mathbf{k}\uparrow}^\dagger c_{-\mathbf{k}\downarrow}^\dagger) |0\rangle, \quad (2)$$

with  $u_{\mathbf{k}}^2 = \frac{1}{2}(1 + \epsilon_{\mathbf{k}} / \sqrt{\epsilon_{\mathbf{k}}^2 + \Delta^2}) = 1 - v_{\mathbf{k}}^2$ ,  $\Delta \geq 0$ , and  $|0\rangle$  is the electronic vacuum [29, 30]. In the projective approach, we define a generalised projector  $\hat{\Pi} = \int_S d\Delta |\Psi(\Delta)\rangle \langle \Psi(\Delta)|$  with which to project out a low-energy circuit Hamiltonian

$$\hat{H} \equiv \hat{\Pi} \hat{H}_{\text{el}} \hat{\Pi} = \int_{S^2} d\Delta d\Delta' H(\Delta, \Delta') |\Psi(\Delta)\rangle \langle \Psi(\Delta')|, \quad (3)$$

where  $H(\Delta, \Delta') = \langle \Psi(\Delta) | \hat{H}_{\text{el}} | \Psi(\Delta') \rangle$  is the Hamiltonian function for the superconducting system.

The BCS basis is normalised,  $\langle \Psi(\Delta) | \Psi(\Delta) \rangle = 1$  (since

$u_{\mathbf{k}}^2 + v_{\mathbf{k}}^2 = 1$ ), but not orthogonal, so  $\hat{\Pi}$  is not idempotent,

$$\hat{\Pi}^2 = \int_{\mathcal{S}^2} d\Delta d\Delta' W(\Delta, \Delta') |\Psi(\Delta)\rangle \langle \Psi(\Delta')| \neq \hat{\Pi}, \quad (4)$$

where  $W(\Delta, \Delta') = \langle \Psi(\Delta) | \Psi(\Delta') \rangle$  is the overlap function.

Electronic eigenstates satisfy  $\hat{H}_{\text{el}}|y\rangle = E|y\rangle$ , and assuming that low-energy eigenstates reside within  $\mathcal{H}_{\text{BCS}}$ , i.e.  $|y\rangle = \int_{\mathcal{S}} d\Delta' y(\Delta') |\Psi(\Delta')\rangle$ , it follows that  $\int_{\mathcal{S}} d\Delta' y(\Delta') \hat{H}_{\text{el}} |\Psi(\Delta')\rangle = E \int_{\mathcal{S}} d\Delta' y(\Delta') |\Psi(\Delta')\rangle$ . This forms a natural superconducting generalisation of the multi-determinant wavefunctions familiar from post-Hartree-Fock methods [31]. Projecting over  $\langle \Psi(\Delta) |$  yields the generalised integral eigenvalue equation

$$\int_{\mathcal{S}} d\Delta' H(\Delta, \Delta') y(\Delta') = E \int_{\mathcal{S}} d\Delta' W(\Delta, \Delta') y(\Delta'). \quad (5)$$

The overlap  $W$  was discussed in [29] as a function of the phase coordinate,  $\phi$ , under the BCS mean-field approximation  $|\Delta| = \Delta_{\text{BCS}} = 2\mathcal{B}e^{-1/\lambda}$  [30], i.e. assuming  $\Delta \in \mathcal{S} = \{\Delta_{\text{BCS}} e^{i\phi}\}_{\phi \in [-\pi, \pi]}$ . That earlier analysis yielded low-energy quantised phase and charge operators  $\hat{\phi}$  and  $\hat{n}$ , as well as standard expressions for quantised superconducting circuit elements which depend on them.

Here, we extend the projective approach to expand the support of the gap parameter from  $\Delta = \Delta_{\text{BCS}}$  to  $\Delta \in \mathbb{R}^+$ . In the expanded ‘gap’ space, we follow a similar analysis to [29], and compute

$$\begin{aligned} W(\Delta, \Delta') &= W(\varphi; \Delta, \Delta'), \\ &\approx e^{n \left( i\frac{\varphi}{2} - \frac{\pi(3(\Delta+\Delta')^2 + 20\Delta\Delta')}{256\mathcal{B}(\Delta+\Delta')} \varphi^2 - \frac{\pi(\Delta-\Delta')^2}{16\mathcal{B}(\Delta+\Delta')} \right)}, \end{aligned} \quad (6)$$

where the dependence on  $\phi$  and  $\phi'$  reduces to the phase-difference,  $\varphi \equiv \phi' - \phi \in [-\pi, \pi)$ . This reduction makes  $W$  *block-circulant* in the phase coordinates, and  $W$  is a Gaussian localised near  $\varphi = 0$ .

The Hamiltonian function is also block-circulant in  $\varphi$ ,

$$\begin{aligned} H(\Delta, \Delta') &= H(\varphi; \Delta, \Delta'), \\ &= (\mathbf{L}(\Delta_+, \Delta_-) + O(\varphi)) W(\varphi; \Delta, \Delta'), \end{aligned} \quad (7)$$

where  $\Delta_{\pm} = (\Delta \pm \Delta')/2$  and the leading,  $\varphi$ -independent term in  $H/W$  is

$$\begin{aligned} \mathbf{L}(\Delta_+, \Delta_-) &= \frac{n}{2\mathcal{B}} \left( \Delta_+^2 \left( -\frac{1}{2} + \ln(2\mathcal{B}/\Delta_+) \right) - \lambda \ln^2(2\mathcal{B}/\Delta_+) \right) \\ &\quad + \Delta_-^2 \left( \frac{2}{3} - \ln(2\mathcal{B}/\Delta_+) \right). \end{aligned} \quad (8)$$

Figure 1 shows the ‘BCS potential’,  $V_{\text{BCS}}(\Delta) \equiv H(0; \Delta, \Delta) \approx \mathbf{L}(\Delta, 0)$ , along the main diagonal  $\Delta' = \Delta$ , attaining a minimum  $-E_{\text{min}} = -n\mathcal{B}e^{-2/\lambda}$  at  $\Delta = \Delta_{\text{BCS}}$ . In mean-field theory, the surface generated by rotating  $V_{\text{BCS}}$  through  $-\pi \leq \phi < \pi$  is the ‘Mexican hat potential’ [17, 29], in which the gap relaxes to  $\Delta_{\text{BCS}}$ .

The block-circulant structure of  $W$  and  $H$  allows simultaneous block-diagonalisation using a discrete Fourier

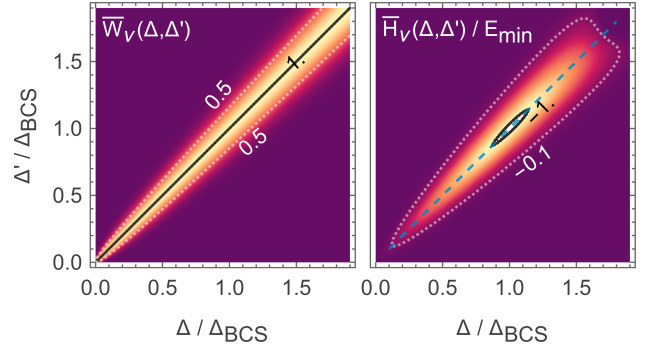


FIG. 2. Normalised Fourier-basis overlap and Hamiltonian functions  $\bar{W}_\nu$  and  $\bar{H}_\nu$  at half-filling, with indicative contours shown. Along the diagonal  $\Delta' = \Delta$  (dashed line),  $\bar{H}_\nu(\Delta, \Delta)$  is qualitatively the same as shown in fig. 1, with a minimum value of  $-E_{\text{min}}$  at  $\Delta = \Delta_{\text{BCS}}$ . For illustrative purposes, we take  $\nu = 0$ ,  $n = 3 \times 10^5$  and  $b = e^{1/\lambda}/2 = 10^3$ .

transform to replace the compact phase coordinate with a conserved island-charge quantum number  $\nu \in \mathbb{Z}$ , chosen so that  $\nu = 0$  corresponds to exact half-filling,

$$\begin{aligned} W_\nu(\Delta, \Delta') &= \int_{-\pi}^{\pi} d\varphi e^{-i(\nu+n/2)\varphi} W(\varphi; \Delta, \Delta'), \\ H_\nu(\Delta, \Delta') &= \int_{-\pi}^{\pi} d\varphi e^{-i(\nu+n/2)\varphi} H(\varphi; \Delta, \Delta'). \end{aligned}$$

Since  $W$  and  $H$  include a narrow Gaussian factor centred at  $\varphi = 0$ , we extend the integration limits to  $\pm\infty$  without significant error. In addition,  $W_\nu$  is unnormalised, which follows because, for circulant overlap matrices, the (unitary) Fourier transform maps the nonortho-normal phase basis to an ortho-nonnormal charge basis [29]. For convenience we normalise in the charge basis by defining

$$\begin{aligned} \bar{W}_\nu(\Delta, \Delta') &= W_\nu(\Delta, \Delta') / N_\nu(\Delta, \Delta'), \\ &= (1 + \Delta_-^2 / (16\Delta_+^2) + O(\nu^2)) e^{-\frac{n\pi\Delta_-^2}{8\mathcal{B}\Delta_+}}, \end{aligned} \quad (9)$$

where  $N_\nu(\Delta, \Delta') = \sqrt{W_\nu(\Delta, \Delta) W_\nu(\Delta', \Delta')}$ , so that  $\bar{W}_\nu(\Delta, \Delta) = 1$ , and

$$\begin{aligned} \bar{H}_\nu(\Delta, \Delta') &= H_\nu(\Delta, \Delta') / N_\nu(\Delta, \Delta'), \\ &= (\mathbf{L}(\Delta_+, \Delta_-) + O(\nu)) \bar{W}_\nu(\Delta, \Delta'). \end{aligned} \quad (10)$$

This normalisation leaves the spectrum invariant, and the integral eigenvalue eq. (5) reduces to

$$\int d\Delta' \bar{H}_\nu(\Delta, \Delta') y_\nu(\Delta') = E \int d\Delta' \bar{W}_\nu(\Delta, \Delta') y_\nu(\Delta'), \quad (11)$$

where the conserved charge  $\nu$  appears parametrically.

Figure 2 shows  $\bar{W}_\nu(\Delta, \Delta')$  and  $\bar{H}_\nu(\Delta, \Delta')$  at half-filling. Qualitatively, these have support near the diagonal  $\Delta = \Delta'$ . Along this main diagonal,  $\bar{H}_\nu(\Delta, \Delta)$  attains a minimum value  $-E_{\text{min}}$  at  $\Delta = \Delta_{\text{BCS}}$ ; this behaviour for a fixed charge  $\nu$  is essentially the same as that for a fixed phase, i.e.  $\bar{H}_\nu(\Delta, \Delta) \approx V_{\text{BCS}}(\Delta)$ , shown in fig. 1.

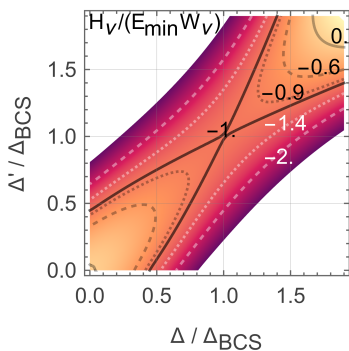


FIG. 3. Illustrating the saddle-point structure in the ratio of the Hamiltonian and overlap functions  $H_\nu(\Delta, \Delta')/W_\nu(\Delta, \Delta')$ , around  $\Delta = \Delta' = \Delta_{\text{BCS}}$ . Parameters are as in fig. 2, with indicative contours shown.

Both  $\bar{W}_\nu$  and  $\bar{H}_\nu$  exhibit a Gaussian decay as a function of the transverse coordinate  $\Delta_-$ . These ‘off-diagonal’ Hamiltonian terms capture the kinetics of the gap mode, which we formalise below. In addition, we note that the ratio  $H_\nu/W_\nu = L + O(\nu)$  exhibits a saddle-point at  $\Delta = \Delta' = \Delta_{\text{BCS}}$ , as illustrated in fig. 3. Analytically, we expand  $L$  in eq. (8) to quadratic order around  $\Delta_+ = \Delta_{\text{BCS}}$  and  $\Delta_- = 0$ , to find

$$L/E_{\text{min}} = (2 - 2/\ln(2b)) (\Delta_+/\Delta_{\text{BCS}} - 1)^2 - 1 - (2\ln(2b) - \frac{4}{3}) (\Delta_-/\Delta_{\text{BCS}})^2 + O(\Delta_\pm^3), \quad (12)$$

where  $b = \mathcal{B}/\Delta_{\text{BCS}} = e^{1/\lambda}/2$  is a dimensionless parameter depending on microscopic quantities. For typical metals,  $\mathcal{B} \gtrsim 1$  eV and  $\Delta_{\text{BCS}} < 1$  meV [32], so  $b \gtrsim 10^3$ . In explicit electron-phonon interaction models the ‘ultraviolet’ cutoff  $\mathcal{B}$  is often replaced by a characteristic phonon frequency  $\bar{\omega}_{\text{ph}} \sim 0.1$  eV [33], so  $b \rightarrow b_{\text{ph}} = \bar{\omega}_{\text{ph}}/\Delta_{\text{BCS}} \gtrsim 10^2$ .

We now extract effective spring and mass constants,  $\kappa_{\text{H}}$  and  $m_{\text{H}}$ , from  $L$  in eq. (12), by comparing it with the Hamiltonian function for a 1D particle of mass  $m$  in a potential  $v(x)$ , with Hamiltonian  $\hat{h} = v(\hat{x}) + \hat{p}^2/(2m)$ . We express  $\hat{h}$  in a normalised, nonorthogonal basis of  $\gamma$ -localised Gaussian wavepackets,  $\{|\psi_{\gamma, \tilde{x}}\rangle\}_{\tilde{x} \in \mathbb{R}}$  with  $\langle x|\psi_{\gamma, \tilde{x}}\rangle = e^{-(x-\tilde{x})^2/(2\gamma^2)}/\sqrt{\pi^{1/2}\gamma}$ , and overlap function

$$\mathbf{w}(\tilde{x}, \tilde{x}') = \langle \psi_{\gamma, \tilde{x}} | \psi_{\gamma, \tilde{x}'} \rangle = e^{-\tilde{x}_-^2/\gamma^2}, \quad (13)$$

where  $\tilde{x}_\pm = (\tilde{x} \pm \tilde{x}')/2$ . For a harmonic potential  $v(x) = \kappa(x - x_0)^2/2 - v_0$  the Hamiltonian function is

$$\begin{aligned} \mathbf{h}(\tilde{x}, \tilde{x}') &= \langle \psi_{\gamma, \tilde{x}} | \hat{h} | \psi_{\gamma, \tilde{x}'} \rangle, \\ &= \mathbf{w}(\tilde{x}, \tilde{x}') (\kappa(\tilde{x}_+ - x_0)^2/2 - v_0 - \tilde{x}_-^2/(2\gamma^4 m) \\ &\quad + \kappa\gamma^2/4 + 1/(4\gamma^2 m)). \end{aligned} \quad (14)$$

As for  $L$ , we see that  $\mathbf{h}/\mathbf{w}$  also has a characteristic saddle-point at  $\tilde{x}_+ = x_0$  and  $\tilde{x}_- = 0$  (i.e. at  $\tilde{x} = \tilde{x}' = x_0$ ), with principal axes aligned along  $\tilde{x}_\pm$ . The  $\kappa$ -dependent (potential) contribution to  $\mathbf{h}/\mathbf{w}$  depends only on  $\tilde{x}_+$ , while

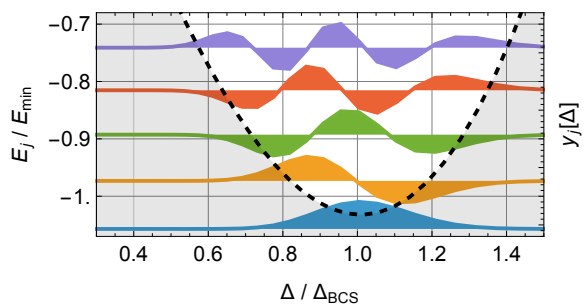


FIG. 4. The lowest five Higgs eigenfunctions,  $y_j(\Delta)$ ,  $j = 0, \dots, 4$ , solved numerically on a discretised grid over  $\Delta$ , and superimposed on the BCS potential (dashed). Eigenfunctions are displaced along the energy axis by their eigenenergy  $E_j$ . Parameters are as in fig. 2.

the mass-dependent (kinetic) contribution depends only on  $\tilde{x}_-$ . Conversely, given functional forms for  $\mathbf{w}$  and  $\mathbf{h}/\mathbf{w}$  we can extract  $\gamma$ ,  $m$ , and  $\kappa$ .

To formally connect to the superconducting gap dynamics, we treat the gap coordinate as a 1D particle in the BCS potential, with minimum at  $\Delta = \Delta_{\text{BCS}}$ . With the correspondence  $\Delta_\pm \leftrightarrow \tilde{x}_\pm$ , we compare the overlap functions  $W_\nu$  and  $\mathbf{w}$  in eqs. (9) and (13), and matching their Gaussian exponents yields

$$\gamma_{\text{H}} = \sqrt{8\mathcal{B}\Delta_{\text{BCS}}/(n\pi)} = \sqrt{8b/(n\pi)}\Delta_{\text{BCS}}. \quad (15)$$

Similarly, matching the coefficients of  $\Delta_\pm^2$  in  $H_\nu/W_\nu \approx L$  in eq. (12), with those of  $\tilde{x}_\pm^2$  in  $\mathbf{h}/\mathbf{w}$  in eq. (14), yields

$$\kappa_{\text{H}}/2 = (2 - 2/\ln(2b))E_{\text{min}}/\Delta_{\text{BCS}}^2, \quad (16)$$

$$1/(2\gamma_{\text{H}}^4 m_{\text{H}}) = (2\ln(2b) - \frac{4}{3})E_{\text{min}}/\Delta_{\text{BCS}}^2. \quad (17)$$

Noting that  $E_{\text{min}} = n\Delta_{\text{BCS}}/(4b)$ , the Higgs frequency is

$$\omega_{\text{H}} = \sqrt{\kappa_{\text{H}}/m_{\text{H}}} \approx \frac{8}{\pi} \sqrt{\ln(2b) - \frac{5}{3}} \Delta_{\text{BCS}}. \quad (18)$$

For  $b > 10^2$ , we find  $\omega_{\text{H}}/\Delta_{\text{BCS}} > 5$ .

In addition, we expect zero-point gap fluctuations around  $\Delta_{\text{BCS}}$  with standard deviation

$$\sigma_{\Delta} = 1/(\kappa_{\text{H}}m_{\text{H}})^{1/4} \approx \ln(2b)^{1/4}\gamma_{\text{H}}. \quad (19)$$

The filled Fermi sea at  $T = 0$  is the quantum state at  $\Delta = 0$  with  $E = 0$ , shown in fig. 1, so bound states are those with  $E < 0$ . In the harmonic approximation, we estimate the number of bound Higgs excitations to be

$$N_{\text{bound}} \approx E_{\text{min}}/\omega_{\text{H}} \approx n\pi/(32b\sqrt{\ln(2b) - 5/3}). \quad (20)$$

Qualitatively, for large system size  $n$ , when  $N_{\text{bound}} \gg 1$ , we anticipate that the lowest eigenmodes will be highly harmonic. Conversely, when  $N_{\text{bound}} \sim 1$ , we expect significant anharmonicity in the low-energy spectrum.

We numerically validate the harmonic analysis above by discretising the gap parameter  $\Delta \rightarrow \Delta_i$ , which corresponds to choosing a discretised set of gap-mode basis

states  $|\Psi_\nu(\Delta_i)\rangle$ . This transforms the integral eigenvalue equation (11) into a generalised matrix eigenvalue problem  $\mathbf{H}\cdot\mathbf{y} = E\mathbf{W}\cdot\mathbf{y}$ , with Hamiltonian and overlap matrices,  $\mathbf{H}$  and  $\mathbf{W}$ , which depend parametrically on  $\nu$ .

For numerics, we use a non-uniform grid over  $\Delta$ , chosen so that  $|\mathbf{W}_{i,i+1}| = |\langle\Psi(\Delta_i)|\Psi(\Delta_{i+1})\rangle| = 1 - \epsilon$ , where  $0 < \epsilon \ll 1$  controls the overlap, independent of  $i$ . For a finely discretised grid, where  $|\Delta_{i+1} - \Delta_i| \ll \gamma_H$ , adjacent gap basis states are highly overlapped, and  $\mathbf{W}$  becomes increasingly ill-conditioned as  $\epsilon \rightarrow 0$ . We find good numerical convergence for  $\epsilon \gtrsim 0.07$ , but for  $\epsilon \lesssim 0.05$  ill-conditioning degrades numerical results.

Figure 4 shows eigenmodes  $y_j(\Delta)$  computed numerically, and displaced along the energy axis by their energy,  $E_j$ . Notably, the ground-state energy is slightly below  $-E_{\min}$ , which is a consequence of the non-orthogonality of the gap-basis. [This is reflected in the constants in the second line of eq. (14), which raise the saddle-value of  $\mathbf{h}$  above  $-v_0$ .] The low-energy generalised eigenfunctions are qualitatively similar to harmonic oscillator modes, with the ground state localised near  $\Delta = \Delta_{\text{BCS}}$ . For the parameters used in fig. 4, eq. (19) gives  $\sigma_\Delta/\Delta_{\text{BCS}} \approx 0.15$ , consistent with the ground-state width shown.

When  $N_{\text{bound}} \gtrsim 2$  we find that the first transition energy matches the Higgs frequency,  $E_{10} \equiv E_1 - E_0 \approx \omega_H$ , as expected. For example, for the parameters used in fig. 4 we find numerically  $E_{10}/E_{\min} = 0.084$ , in agreement with  $\omega_H/E_{\min} = 1/N_{\text{bound}} = 0.083$  from eq. (20).

Figure 5 shows  $E_{10}$  computed numerically (circles), and  $\omega_H$  from eq. (18) (solid line), against the dimensionless bandwidth,  $b$ . The logarithmic dependence  $\omega_H/\Delta_{\text{BCS}} \approx \frac{8}{\pi} \sqrt{\ln(2b)} > 5$  for small islands exceeds the long-wavelength prediction of  $\omega_H/\Delta_{\text{BCS}} \approx 2$  [15, 17]. We understand this difference arises from the quasi-zero-dimensional limit we consider, where the system size is smaller than the superconducting coherence length.

Figure 5 also shows the ‘quantum’ anharmonicity,  $\alpha_{210} = E_{10} - E_{21}$  (squares) computed numerically for  $n = 10^5$  and  $10^6$ , showing frequency softening, and empirically scales as  $\alpha_{210} \propto b \ln(2b)/n$ . Larger systems have smaller anharmonicity, as expected, while  $\alpha_{210}$  can be an appreciable fraction of  $\omega_H$  for small systems.

The cubic potential contribution to  $\mathbf{L}$  in eq. (8) is  $V_{\text{BCS}}^{(3)} = E_{\min} \chi (\Delta_+/\Delta_{\text{BCS}} - 1)^3$ , where  $\chi = 2/3 - 2/\ln(2b)$ , giving rise to second-order perturbative energy shifts. These contribute an anharmonic shift  $\alpha_{210}^{(3)} = \frac{15 \sigma_\Delta^6}{2 \omega_H} \left(\frac{E_{\min} \chi}{\Delta_{\text{BCS}}^3}\right)^2 \approx 40 b \ln(2b)/(3n\pi^2)$ . The functional dependence on  $n$  and  $b$  in  $\alpha_{210}^{(3)}$  agrees with the numerical behaviour of  $\alpha_{210}$ , but quantitatively underestimates it by a factor  $\approx 15$ . We attribute this to (a) higher-order potential contributions, and (b) the dependence of  $m_H$  on  $\Delta_+$  which localises excited eigenmodes, increasing the wavefunction overlaps that contribute to anharmonic perturbations.

Using aluminium as an example,  $\Delta_{\text{BCS}} = 340 \mu\text{eV} =$

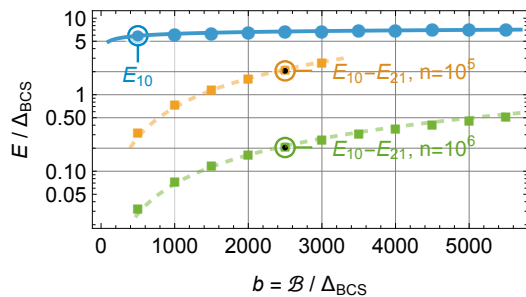


FIG. 5. The first excitation transition energy  $E_{10} \equiv E_1 - E_0$  computed numerically (circles) is in close agreement with the Higgs frequency  $\omega_H$  (solid line, eq. (18)), as a function of the dimensionless bandwidth  $b$ ;  $E_{10}$  is essentially independent of system size  $n$ . We also show the anharmonicity,  $\alpha_{210} = E_{10} - E_{21}$  (squares), for  $n = 10^5$  and  $10^6$ . Larger systems are less anharmonic. Dashed curves are the semi-analytic expression  $15 \alpha_{210}^{(3)}$ , based on perturbative shifts.

82 (2 $\pi$  GHz) and  $\mathcal{B} = 11$  eV [34], so  $b \approx 3 \times 10^4$ . Equation (18) predicts a Higgs frequency of  $\omega_H \approx 7.8 \Delta_{\text{BCS}}$ , so  $\omega_H \approx 640$  (2 $\pi$  GHz). For  $n = 10^7$ , we compute  $\alpha_{210} \approx 0.35 \Delta_{\text{BCS}} = 28$  (2 $\pi$  GHz). Aluminium has a 4-atom face-centred cubic unit cell of side length  $l_c = 0.4$  nm, so at half-filling  $n = 10^7$  would correspond to a cubic island of side length  $l = n^{1/3} l_c / 2 \approx 43$  nm. This suggests promising experimental directions for observing a superconducting Higgs transition in the near-THz band, that, for moderately small isolated islands, would have an appreciable quantum anharmonicity.

To conclude, the analysis presented here extends the projective approach to circuit quantisation [28, 29] to include anharmonic Higgs excitations, expanding superconducting circuit theory beyond the ground-state Higgs-mode manifold. We have focused on the physics of a small island, whose Hilbert space is parameterised by a single complex coordinate  $\Delta$ , but this can be expanded to spatially delocalised systems. Our results suggest an exciting direction in superconducting electronics that uses the intrinsic anharmonicity of superconducting Higgs modes of small islands to encode and manipulate quantum information, akin to the two-band superconductor proposed by Leggett [35]. With near-THz transition frequencies, and anharmonicities  $\gtrsim 10$  GHz in nanometer-scale electronics, compact superconducting qubit systems may be feasible, with correspondingly high operating frequencies and temperatures. Key to developing this direction is understanding the relaxation mechanisms and lifetimes of Higgs modes, and the complementary task of practical control of such devices.

The authors acknowledge funding from the Australian Research Council Centre of Excellence for Engineered Quantum Systems CE170100009, and thank S. Barrett and A. Doherty for formative discussions.

---

\* [yunchih.liao@uq.edu.au](mailto:yunchih.liao@uq.edu.au)

† [stace@physics.uq.edu.au](mailto:stace@physics.uq.edu.au)

- [1] P. W. Higgs, *Phys. Rev. Lett.* **13**, 508 (1964).
- [2] Y. Nambu, *Phys. Rev.* **117**, 648 (1960).
- [3] P. W. Anderson, *Phys. Rev.* **130**, 439 (1963).
- [4] J. Bardeen, L. N. Cooper, and J. R. Schrieffer, *Phys. Rev.* **108**, 1175 (1957).
- [5] P. W. Anderson, *Phys. Rev.* **112**, 1900 (1958).
- [6] P. B. Littlewood and C. M. Varma, *Phys. Rev. Lett.* **47**, 811 (1981).
- [7] N. N. Bogoljubov, V. V. Tolmachov, and D. V. Širkov, *Fortschritte der Physik* **6**, 605 (1958).
- [8] V. L. Ginzburg and L. D. Landau, *Zh. Eksp. Teor. Fiz.* **20**, 1064 (1950).
- [9] R. A. Barankov, L. S. Levitov, and B. Z. Spivak, *Phys. Rev. Lett.* **93**, 160401 (2004).
- [10] E. A. Yuzbashyan, O. Tsypliyatyev, and B. L. Altshuler, *Phys. Rev. Lett.* **96**, 097005 (2006).
- [11] A. F. Volkov and S. M. Kogan, *Zh. Eksp. Teor. Fiz.*, v. 65, no. 5, pp. 2038-2046 (1973).
- [12] E. A. Yuzbashyan, B. L. Altshuler, V. B. Kuznetsov, and V. Z. Enolskii, *Phys. Rev. B* **72**, 220503 (2005).
- [13] H. Krull, D. Manske, G. S. Uhrig, and A. P. Schnyder, *Phys. Rev. B* **90**, 014515 (2014).
- [14] M. H. S. Amin, E. V. Bezuglyi, A. S. Kijko, and A. N. Omelyanchouk, *Low Temperature Physics* **30**, 661 (2004).
- [15] T. Kuhn, B. Sothmann, and J. Cayao, *Phys. Rev. B* **109**, 134517 (2024).
- [16] R. Shimano and N. Tsuji, *Annual Review of Condensed Matter Physics* **11**, 103 (2020).
- [17] P. B. Littlewood and C. M. Varma, *Phys. Rev. B* **26**, 4883 (1982).
- [18] R. Sooryakumar and M. V. Klein, *Phys. Rev. Lett.* **45**, 660 (1980).
- [19] R. Sooryakumar and M. V. Klein, *Phys. Rev. B* **23**, 3213 (1981).
- [20] R. Matsunaga, Y. I. Hamada, K. Makise, Y. Uzawa, H. Terai, Z. Wang, and R. Shimano, *Phys. Rev. Lett.* **111**, 057002 (2013).
- [21] R. Matsunaga, N. Tsuji, H. Fujita, A. Sugioka, K. Makise, Y. Uzawa, H. Terai, Z. Wang, H. Aoki, and R. Shimano, *Science* **345**, 1145 (2014), <https://www.science.org/doi/pdf/10.1126/science.1254697>.
- [22] D. Sherman, U. S. Pracht, B. Gorshunov, S. Poran, J. Jesudasan, M. Chand, P. Raychaudhuri, M. Swanson, N. Trivedi, A. Auerbach, M. Scheffler, A. Frydman, and M. Dressel, *Nature Physics* **11**, 188 (2015).
- [23] T. E. Glier, S. Tian, M. Rerrer, L. Westphal, G. Lüllau, L. Feng, J. Dolgner, R. Haenel, M. Zonno, H. Eisaki, M. Greven, A. Damascelli, S. Kaiser, D. Manske, and M. Rübhausen, *Nature Communications* **16**, 7027 (2025).
- [24] Y. Wang, I. Petrides, G. McNamara, M. M. Hosen, S. Lei, Y.-C. Wu, J. L. Hart, H. Lv, J. Yan, D. Xiao, J. J. Cha, P. Narang, L. M. Schoop, and K. S. Burch, *Nature* **606**, 896 (2022).
- [25] U. Vool and M. Devoret, *International Journal of Circuit Theory and Applications* **45**, 897 (2017), <https://onlinelibrary.wiley.com/doi/pdf/10.1002/cta.2359>.
- [26] D. T. Le, A. Grimsmo, C. Müller, and T. M. Stace, *Phys. Rev. A* **100**, 062321 (2019).
- [27] D. Thanh Le, J. H. Cole, and T. M. Stace, *Phys. Rev. Res.* **2**, 013245 (2020).
- [28] A. Mizel, *Phys. Rev. Appl.* **21**, 024030 (2024).
- [29] Y.-C. Liao, B. J. Powell, and T. M. Stace, *Phys. Rev. Res.* **7**, 033144 (2025).
- [30] J. Annett, *Superconductivity, Superfluids and Condensates*, Oxford Master Series in Physics (OUP Oxford, 2004).
- [31] P. Fulde, *Electron Correlations in Molecules and Solids* (Springer, Berlin Heidelberg, 1995).
- [32] D. H. Douglass and R. Meservey, *Phys. Rev.* **135**, A19 (1964).
- [33] R. Dynes, *Solid State Communications* **10**, 615 (1972).
- [34] H. J. Levinson, F. Greuter, and E. W. Plummer, *Phys. Rev. B* **27**, 727 (1983).
- [35] A. J. Leggett, *Progress of Theoretical Physics* **36**, 901 (1966), <https://academic.oup.com/ptp/article-pdf/36/5/901/5256693/36-5-901.pdf>.